Fluorinated boron nitride nanosheets as an inorganic matrix for the MALDI mass spectrometry analysis of perfluoroalkyl acids

Yanfang Zhao, Huizhi Li, Guiju Xu, Rabah Boukherroub, Xiang Yu, Xiangfeng Chen

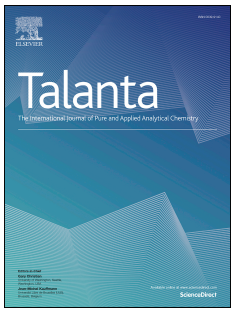

Fluorinated boron nitride nanosheets as an inorganic matrix for the MALDI mass spectrometry analysis of perfluoroalkyl acids

Yanfang Zhao, Huizhi Li, Guiju Xu, Rabah Boukherroub, Xiang Yu, Xiangfeng Chen

PII: S0039-9140(22)00161-8

DOI: https://doi.org/10.1016/j.talanta.2022.123365

Reference: TAL 123365

To appear in: *Talanta*

Received Date: 24 December 2021

Revised Date: 28 February 2022

Accepted Date: 3 March 2022

Please cite this article as: Y. Zhao, H. Li, G. Xu, R. Boukherroub, X. Yu, X. Chen, Fluorinated boron nitride nanosheets as an inorganic matrix for the MALDI mass spectrometry analysis of perfluoroalkyl acids, *Talanta* (2022), doi: https://doi.org/10.1016/j.talanta.2022.123365.

Credit Author Statement

Yanfang Zhao: conceptualization, methodology, formal analysis, and original draft preparation; Huizhi Li: methodology, data analysis, and software preparation; Guiju Xu: investigation, experiment of sample pretreatment, and methodology; Rabah Boukherroub: writing- review &editing; Xiang Yu: project administration, validation, and review; Xiangfeng Chen: conceptualization, draft review, and language editing.

Graphical abstract

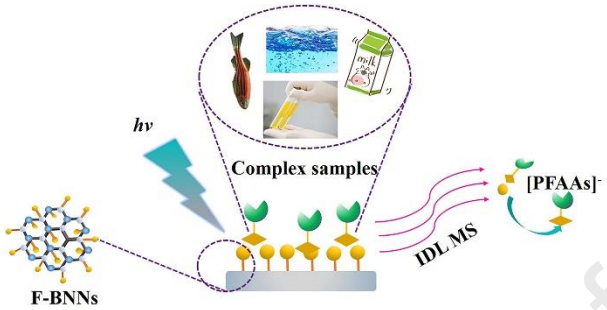

Fluorinated hexagonal boron nitride nanosheets (F-BNNs) was first used as an inorganic matrix for matrix-assisted laser desorption and ionization mass spectrometry (MALDI MS) analysis of perfluoroalkyl acids (PFAAs) in complex samples in negative reflector mode.

Fluorinated Boron Nitride Nanosheets as an Inorganic Matrix for the MALDI Mass Spectrometry Analysis of Perfluoroalkyl Acids

Yanfang Zhao,[a,b] Huizhi Li,[b] Guiju Xu,[b] Rabah Boukherroub,[c] Xiang Yu,*[,a] Xiangfeng Chen,*[,b]

[a]*Beijing Key Laboratory of Materials Utilisation of Nonmetallic Minerals and Solid Wastes, National Laboratory of Mineral Materials, School of Materials Science and Technology, China University of Geosciences, Beijing 100083, PR China.*

[b]*Key Laboratory for Applied Technology of Sophisticated Analytical Instruments of Shandong Province, Shandong Analysis and Test Centre, Qilu University of Technology (Shandong Academy of Sciences), Jinan, Shandong, 250014, PR China.*

[c]*Univ. Lille, CNRS, Centrale Lille, Univ. Polytechnique Hauts-de-France, UMR 8520, IEMN, F-59000 Lille, France*

Abstract

We report, for the first time, the application of fluorinated hexagonal boron nitride nanosheets (F-BNNs) as an effective inorganic matrix for matrix-assisted laser desorption and ionization mass spectrometry (MALDI-MS) analysis of perfluoroalkyl acids (PFAAs). Fluoride modification of F-BNNs increases both enrichment ability and ionization efficiency. The method was validated using environmental water, milk, human serum samples, and zebrafish imaging that has been previously exposed to PFAAs. The method provided in this work holds considerable promise in term of rapid analysis, sample requirement, and practicability.

Keywords: Fluorinated hexagonal boron nitride nanosheets; Inorganic matrix; Perfluoroalkyl acids; Fluorine–fluorine interactions; MALDI-MS; Imaging

1. Introduction

Matrix-assisted laser desorption and ionization mass spectrometry (MALDI-MS) has been developed into a convenient and sensitive strategy for analyzing various molecules in complex samples [1,2]. Organic matrices, including sinapic acid (SA), 2,5-dihydroxybenzoic acid (DHB) and α-cyano-4-hydroxycinnamic acid (CHCA), are usually employed by MALDI-MS [3,4]. However, these matrices commonly produce high background noise in the low molecular weight range (m/z<600), which may limit their application for the detection of various small molecules [5-7].

To overcome these limitations, extensive efforts have been devoted to the development of various organic molecules, such as 3,4-dimethoxycinnamic acid (DMCA) [8], 3-aminophthalhydrazide (3-APH) [9], and 2,3,4,5-tetrakis (3′,4′-dihydroxylphenyl) thiophene (DHPT) [10], for use as MALDI-MS matrices. Nanomaterials, including carbon materials [11-13], silicon-based materials [14,15], metal-containing nanomaterials [16,17], and covalent organic frameworks [18,19] have been successfully applied as inorganic matrices to enhance the signal-to-noise ratio of MALDI-MS and expand its application.

Specifically, boron nitride nanosheets (BNNs) have demonstrated great potential as a MALDI matrix, owing to its similarity to graphene, namely its atomic arrangement and electron configuration [20]. It is weel-estabilished that the shape/size of nanomaterials may affect the spectroscopic signal [21,22]. Therefore, the large nanosheets of boron nitride, featuring a high density of active sites, are favorable in enhancing tis performance in MALDI-MS analysis. Moreover, both the large specific surface area (SSA) and polarity of the B–N bond enable BNNs to easily adsorb other molecules *via* weak interactions [23,24]. The proton transporter with a structure comprising B–H six-membered rings is expected to help in ionizing analytes during the MALDI process. Fluorinated hexagonal boron nitride nanosheets (F-BNNs) are an important derivative of BNNs [25,26]. Unlike BNNs, the F atoms provide much opportunities to adsorb and enrich other fluorinated compounds via fluorine–fluorine interactions [27].

It is noteworthy that fluoride modification can significantly reduce the agglomeration of BNNs, providing them with good dispersibility in water to assist the LDI process.

Perfluoroalkyl acids (PFAAs) are a class of synthetic organic pollutants with carbon skeletons whose hydrogen atoms are replaced by fluorine atoms [28,29]. PFAAs are widely applied in industrial manufacturing and consumer goods due to their special properties originating from their fluorine atoms. PFAAs screening is significantly important to the studies of environmental development and public health [30]. To date, high-performance liquid chromatography coupled with tandem mass spectrometry (HPLC-MS/MS) is the primary method in detecting PFAAs in complex samples [31,32]. However, such methods require complicated, and laborious sample preparation procedures.

In this study, porous F-BNNs substrate was prepared and employed as an efficient platform to improve the MALDI-MS analysis of PFAAs, for the first time. We demonstrated that F-BNNs exhibit better MALDI-MS performance in negative-ion mode than traditional organic matrices and carbon-based materials. Furthermore, high sensitivity and good reproducibility were achieved when the F-BNNs were used as an adsorbent of PFAAs and MALDI-MS matrix. Notably, the method allowed successful detection of PFAAs in environmental water, milk, and human serum samples. Moreover, MALDI-MS imaging (MSI) using the F-BNNs matrix revealed the distribution of PFAAs in zebrafish after their exposure to these chemicals. These results demonstrate that F-BNNs is an effective matrix for MALDI-MS analysis of PFAAs in complex environmental and biological samples. Fig. 1 illustrates the synthesis of the F-BNNs and its application.

2. Experimental

2.1 Chemicals

PFAAs included perfluorobutanoic acid (PFBA), perfluorobutanesulfonic acid (PFBS), perfluorohexanoic acid (PFHxA), perfluoroheptanoic acid (PFHpA), perfluorohexanesulfonate (PFHxS), perfluorooctanoic acid (PFOA), perfluorononanoic acid (PFNA), perfluorooctanoic sulfonic acid (PFOS),

perfluorodecanoic acid (PFDA), and perfluoroundecanoic acid (PFUnA). The details of chemicals and other regents are provided in the Supporting Information.

2.2 Preparation of F-BNNs matrix

The BNNs were synthesized using a modified literature method [33]. The BNNs were then fluorinated *via* a one-step process employing ammonium fluoride [34]. The chemicals, characterization methods, and detailed synthetic procedures are described in the Supporting Information.

2.3 Sample preparation

The details of sample preparation procedure are described in the Supporting Information.

2.4 MALDI-MS analysis

A Bruker rapiflex TOF mass spectrometer (Bruker, Bremen, Germany) was employed to conduct MALDI experiments. Sample measurements were recorded in negative reflector mode within a mass range of *m/z* 200–600. All the mass spectra were acquired using flexControl software (version 3.4) provided by the manufacturer. The obtained MS data were analysed by Flex Analysis 4.0, and MSI results were analysed by Scils 2018b software (Bruker, Bremen, Germany). The other instrumental parameters are described in the Supporting Information.

3. Results and discussion

3.1 Characterization of F-BNNs

Scanning electron microscopy (SEM) image of the F-BNNs (Fig. 2a) showed a 2D layered structure with extensive wrinkles, which was further confirmed by transmission electron microscopy (TEM) (Fig. 2b) imaging. X-ray photoelectron spectroscopy (XPS) (Fig. 2c) was carried out to identify the related elements and chemical composition of the F-BNNs. The B 1s, N 1s, and O 1s were observed at binding energies of 190.5, 397.9, and 532.1 eV, respectively. As expected, a peak at 686.9 eV corresponding to F 1s was evidenced for the F-BNNs, but not for the un-modified BNNs. In addition, C 1s peaks were observed in both the BNN and F-BNNs XPS spectra, which may be ascribed to the carbon coating

employed during XPS test procedure. The F 1s fine spectrum (Fig. 2d) of the F-BNNs indicated their successfully modification with fluoride. The B 1s fine spectrum in the F-BNNs (Fig. 2e) is deconvoluted into three peaks corresponding to B−N, B−F, and B−O bonds at 190.3, 191.0, and 192.0 eV, respectively. The binding energies of the B−F and B−N bonds are in good agreement with a previous study on F-BNNs obtained *via* a hydrothermal reaction method [34]. Notably, the presence of B−F bond signal in the B 1s XPS spectrum further confirmed the successful fluorine-functionalization [35]. The N 1s fine spectrum of the F-BNNs (Fig. 2f) exhibited a main peak at 397.9 eV due to N−B bonds, and a peak at around 398.7 eV ascribed to N−F bonds. The BNNs and F-BNNs were subsequently evaluated by X-ray diffraction (XRD) (Fig. 2g). The XRD pattern of BNNs possessed a wide diffraction peak at 25.3° and another peak at 42.5° assigned the (002) and (100) planes of BNNs, respectively. The ordered in-plane characteristics of the BNNs were clearly altered by fluorine-functionalization [36]; for instance, the disappearance of the (100) diffraction peak at 42.5° in the F-BNNs pattern obviously indicated that fluorine-functionalization caused a collapse of the crystal structure of BNNs. The FTIR spectra of BNNs and F-BNNs (Fig. 2h) displayed a strong band at 1379.2 cm^{-1} ascribed to B−N stretching. Moreover, the sharp band at 804.1 cm^{-1} was assigned to the B−N−B out-of-plane bending mode [37]. Additionally, a B−F vibrational feature was reflected by the presence of two weak peaks at around 1265.2 and 1075.2 cm^{-1}, respectively. The F-BNNs' SSA was determined to be 798.1 m^2/g (Fig. 2i), and the pore size was 3.5 nm (Fig. 2i insert). The optical properties of F-BNNs were assessed during UV-vis absorption spectrophotometry. A strong and wide (300 to 700 nm) optical absorption was observed (Fig. S1); this feature is beneficial for its application as an inorganic matrix to absorb efficiently the incoming laser energy and then transfer it to target molecules to achieve their desorption/ionization and analysis by MALDI-MS [18].

3.2 Comparative study of the desorption/ionization of PFAAs

F-BNNs exhibited a clean background (Fig. S2) in low-mass region. The performance of the F-BNNs as a MALDI matrix was compared to that of other traditional organic matrices and graphene-based materials, including CHCA, DHB, BNNs, graphene oxide (GO), and graphene sheets (GS). As shown in Fig. 3a, ten deprotonated $[M-H]^-$ ions of PFAAs were detected using the F-BNNs matrix. The *m/z* peaks at 213.03, 299.10, 313.05, 363.06, 399.11, 413.07, 463.08, 499.13, 512.94, and 563.09 were assigned to $[PFBA-H]^-$, $[PFBS-H]^-$, $[PFHxA-H]^-$, $[PFHpA-H]^-$, $[PFHxS-H]^-$, $[PFOA-H]^-$, $[PFNA-H]^-$, $[PFOS-H]^-$, $[PFDA-H]^-$, $[PFUnA-H]^-$ species, respectively. In contrast, the BNNs (Fig. 3b), CHCA (Fig. 3c), DHB (Fig. 3d), GO (Fig. 3e), and GS (Fig. 3f) matrices only detected seven, five, four, three, and three analytes, respectively. Moreover, the relative mass peak intensities of the analytes detected with the F-BNNs matrix were higher than those recorded using the other matrices. These results demonstrate that the F-BNNs effectively increased the desorption/ionization efficiencies of small molecules.

3.3 Salt tolerance and repeatability of F-BNNs as a MALDI matrix

The salt tolerance experiments in supporting information were conducted for the analysis of various aqueous solutions of PFHxS in presence of increasing concentration of NaCl (0-500 mM). When NaCl concentration reached 500 mM, the mass peak intensity of PFHxS decreased to 84.5% of the initial value (Fig. 4a), demonstrating the strong salt tolerance of F-BNNs as an inorganic matrix. The relative standard deviations (RSDs) of shot-to-shot and spot-to-spot for PFAAs were 6.72-11.3% and 7.33-12.6%, respectively (Table S1). Furthermore, six batches of F-BNNs were prepared to study the reproducibility of the synthetic method. As presented in Table S2, the batch-to-batch assay varied from 2.99% to 13.4%, which clearly demonstrates the good reproducibility performance owing to the uniform distribution of F-BNNs.

3.4 Possible interaction mechanism between F-BNNs and PFAAs

The electronic transition mechanism provided a significant influence in desorption/ionization of PFAAs. Upon laser light adsorption, electrons were

emitted from F-BNNs, followed by their subsequent interaction with PFAAs to produce $[M-H]^-$ [38]. The superior performance of the F-BNNs can be attributed to its unique structural characteristics and the possible ionization mechanism, which can be summarized as follows: (i) The fluorine atoms of the F-BNNs provide a great affinity for PFAAs based on fluorine–fluorine interactions [35]. The F-BNNs could, therefore, effectively adsorb numerous fluorinated analytes *via* fluorine affinity. (ii) The fluorine atoms of the F-BNNs also enhance the affinity for analytes by providing sites for hydrophobic interactions and hydrogen bonding, thus improving the ionization efficiencies of the target molecules [39]. (iii) Fluoride modification can improve the dispersibility of the F-BNNs in water; homogeneous F-BNNs can offer satisfactory reproducibility [40].

3.5 Method validation and analysis of PFAAs in real samples

To evaluate the ability of the F-BNNs as an effective adsorbent and matrix for MALDI-MS, it was applied for PFAAs detection in water (Table S3). The limit of detection (LOD) of PFAAs was determined by spotting of a series of diluted standard solution which were enriched by F-BNNs on a stainless MALDI target plate until corresponding to signal-to-noise (S/N) ratio of three was obtained. Linearity of the proposed method was evaluated for PFAAs mixed standard solutions with a series of concentrations (0.3-500 μg L^{-1}). MALDI-MS analysis was performed according to the parameters described in the section of 2.3 and Supporting Information. The limit of detection (LOD, signal to noise, S/N=3) of the matrix for the PFAAs analytes was 0.08–0.2 μg L^{-1}, the linear range was 0.3–500 μg L^{-1}, and the correlation coefficient (r) was between 0.9841 and 0.9955. Compared to blank water (Fig. S3a), ten PFAAs were clearly detected in the spectrum after spiking the water with 5 μg L^{-1} of PFAAs (Fig. S3b). The reproducibility study was performed by parallel analysis of RSDs of the shot-to-shots and sample-to-sample RSDs. The reproducibility RSD of the shot-to-shot was 7.56–14.6%, and sample-to-sample RSD was 5.35–12.5%. The method was then used to investigate PFAAs detection in wastewater; specifically, PFOS (0.33 μg L^{-1}) was found in leather wastewater (Fig. S3c), PFBS (0.22 μg L^{-1}) was

detected in dyeing wastewater, and PFHxS was measured in both leather (0.13 μg L^{-1}) and dyeing (0.12 μg L^{-1}) wastewater (Fig. S3d).

In addition, the method was used to investigate the analytes in milk (Table S4). The LODs of PFAAs were 0.15–1.5 μg L^{-1}, the linear dynamic range was 0.2–500 μg L^{-1}, and the *r* ranged from 0.9878 to 0.9975. The reproducibility RSD of the shot-to-shot was 6.39–14.5%, and sample-to-sample RSD was 6.38–14.7% was obtained. The mass spectrum obtained without the F-BNNs matrix (Fig. S4a) showed no PFAAs in the milk samples, unless they were purposely spiked samples. In contrast, all ten PFAAs were successfully detected in the presence of the F-BNNs matrix (Fig. S4b), proving that the FBNNs can effectively serve as an enrichment and ionization matrix for the MALDI-MS detection of PFAAs in milk samples.

To further study the performance of the F-BNNs matrix in quantitative analysis, PFAAs in human serum samples were determined by using the developed method. The spectra collected before (Fig. 4b) and after (Fig. 4c) PFAAs (5 μg L^{-1}) enrichment were compared, with the peaks of six PFAAs being clearly observed in the latter. The PFAAs linear detection range was from 2 to 500 μg L^{-1}, and the *r* was between 0.9788 and 0.9963 (Table S5). The LODs was 0.14–1.50 μg L^{-1}. The reproducibility RSDs toward shot-to-shot was 8.32–13.6%, and sample-to-sample RSDs was between 7.62% and 13.5%.

The F-BNNs showed a homogeneous substance (Fig. S5), and were used as a matrix for MALDI-MSI analysis of zebrafish exposed to PFAAs, where the spatial distribution of the PFAAs was clearly revealed (Fig. 4d). The PFAAs primarily accumulated around the eyes, liver, sexual organs, anus, and end of sex organ. The distribution of PFAAs in the eyes may be due to the eyes being exposed to the outside environment. Meanwhile, the PFAAs in the liver could be detected because the liver, as a detoxification organ, easily transports and metabolizes exogenous pollutants. Furthermore, some of the perfluorinated compounds were metabolized by the body and entered the anus and reproductive organs. The results showed that F-BNNs can be used as a matrix for MALDI-

MSI, which could provide spatial distribution information in zebrafish exposed to PFAAs. The distribution of target exposed at the same concentration for fish could not be detected with conventional organic substrate.

4. Conclusion

In summary, F-BNNs matrix was successfully applied in MALDI-MS and MSI analysis of PFAAs in complex samples. Compared with both organic (CHCA, DHB) and inorganic (GO, GS and pure BNNs) matrices, the F-BNNs showed minimal background interference and high sensitivity. F-BNNs matrix exhibited good salt tolerance and high reproducibility. Fluoride modification facilitated extraction and ionization efficiency. The detailed mechanism by which the F-BNNs assisted desorption/ionization process needs to be further studied. It is expected that this work can serve as a foundation for the F-BNNs-assisted MALDI-MS detection of other perfluorinated molecules in complex environmental and biological samples.

Acknowledgment

This work was supported by the Shandong Provincial Key Research and Development Program (Major Scientific and Technological Innovation Project) (No. 2019JZZY020903), the National Natural Science Foundation of China (No. 22074071, 22106080, 51571183), and the Program for Taishan Scholars of Shandong Province (NO. tsqn 202103099, X. Chen).

References

[1] H.Y. Xie, R. Wu, Y.L. W. Huang, X.F. Chen, T.-W. Dominic Chan, Development of a matrix sublimation device with controllable crystallization temperature for MALDI mass spectrometry imaging, Anal. Chem. 93 (2021) 6342–6347.

[2] J. Wang, Q. Liu, Y. Gao, Y.W. Wang, L.Q. Guo, G.B. Jiang, High-throughput and rapid screening of low-mass hazardous compounds in complex samples, Anal. Chem. 87 (2015) 6931–6936.

[3] C.X. Yang, H.K. Lee, Y.H. Zhang, L-L. Jiang, Z-F. Chen, C.K. Chung, Z.W. Cai, *In situ* detection and imaging of PFOS in mouse kidney by matrix-assisted laser desorption/ionization imaging mass spectrometry, Anal. Chem. 91 (2019) 8783–8788.

[4] P.F. Wu, Y.Y. Tang, G.D. Cao, J.P. Li, S.Q. Wang, X.Y. Chang, M. Dang, H.B. Jin, C.M. Zheng, Z.W. Cai, Determination of environmental micro(nano)plastics by matrix-assisted laser desorption/ionization-time-of-flight mass spectrometry, Anal. Chem. 92 (2020) 14346–14356.

[5] C.C. Chen, S.R. Laviolette, S.N. Whitehead, J.B. Renaud, K.K.C. Yeung, Imaging of neurotransmitters and small molecules in brain tissues using laser desorption/ionization mass spectrometry assisted with zinc oxide nanoparticles, J. Am. Soc. Mass. Spectrom. 32 (2021)

1065–1079.
[6] C.X. Ma, X. Wang, H.M. Zhang, W. Liu, D.J. Wang, F. Liu, H. Lu, L.Q. Huang, High-throughput screening and spatial profiling of low-mass pesticides using a novel Ti_3C_2 MXene nanowire (TMN) as MALDI-MS matrix, Chemosphere 286 (2022) 131826.
[7] C.L. Sun, W. Liu, Y. Mu, X. Wang, 1,1′-binaphthyl-2,2′-diamine as a novel MALDI matrix to enhance the *in-situ* imaging of metabolic heterogeneity in lung cancer, Talanta 209 (2020) 120557.
[8] H.X. He, L. Qin, Y.W. Zhang, M.M. Han, J.M. Li, Y.Q. Liu, K.D. Qiu, X.Y. Dai, Y.Y. Li, M.M. Zeng, H.H. Guo, Y.J. Zhou, X.D. Wang, 3,4-Dimethoxycinnamic acid as a novel matrix for enhanced *in-situ* detection and imaging of low-molecular-weight compounds in biological tissues by MALDI-MSI, Anal. Chem. 91 (2019) 2634–2643.
[9] B. Li, R.Y. Sun, A. Gordon, J.Y. Ge, Y. Zhang, P. Li, H. Yang, 3-aminophthalhydrazide (luminol) as a matrix for dual-polarity MALDI-MS imaging, Anal. Chem. 91 (2019) 8221–8228.
[10] Z. Qiao, F. Lissel, MALDI matrices for the analysis of low molecular weight compounds: rational design, challenges and perspectives, Chem. Asian. J. 16 (2021) 868-878.
[11] S.-W. Kim, S.B. Kwon, Y.K. Kim, Graphene oxide derivatives and their nanohybrid structures for laser desorption/ionization time-of-flight mass spectrometry analysis of small molecules, Nanomaterials 11 (2021) 288.
[12] L.Y. Lu, G.C. Zheng, M. Wang, D.D. Wang, Z.N. Xia, Microwave-prepared mesoporous graphene as adsorbent and matrix of surface-assisted laser desorption/ionization mass spectrometry for the enrichment and rapid detection of polyphenols in biological samples. Talanta 222 (2021) 121365.
[13] N. Li, S.M. Li, T. Li, H. Yang, Y.Y. Zhang, Z.W. Zhao, Co-incorporated mesoporous carbon material-assisted laser desorption/ionization ion source as an online interface of in vivo microdialysis coupled with mass spectrometry, Anal. Chem. 92 (2020) 5482–5491.
[14] X.-N. Wang, W.W. Tang, A. Gordon, H.-Y. Wang, L.R. Xu, P. Li, B. Li, Porous TiO_2 film immobilized with gold nanoparticles for dual-polarity SALDI MS detection and imaging, ACS Appl. Mater. Interfaces 12 (2020) 42567–42575.
[15] J. Wu, D. Ouyang, Y.T. He, H. Su, B.C. Yang, J. Li, Q.Q. Sun, Z. Lin, Z.W. Cai, Synergistic effect of metal-organic framework/gallic acid in enhanced laser desorption/ionization mass spectrometry, ACS Appl. Mater. Interfaces 11 (2019) 38255–38264.
[16] W.-W. Wei, Y.H. Zhong, T. Zou, X.-F. Chen, L. Ren, Z.H. Qi, G.G. Liu, Z.-F. Chen, Z.W. Cai, Fe_3O_4-assisted laser desorption ionization mass spectrometry for typical metabolite analysis and localization: Influencing factors, mechanisms, and environmental applications, J. Hazard. Mater. 388 (2020) 121817.
[17] Y.L. Zhu, Y.M. Lian, J.K. Wang, Z.P. Chen, R.-Q. Yu. Ultrasensitive detection of protein biomarkers by MALDI-TOF mass spectrometry based on $ZnFe_2O_4$ nanoparticles and mass tagging signal amplification, Talanta 224 (2021) 121848.
[18] K. Hu, Y.X. Lv, F.G. Ye, T. Chen, S. Zhao, Boric-acid-functionalized covalent organic framework for specific enrichment and direct detection of cis-diol-containing compounds by matrix-assisted laser desorption/ionization time-of-flight mass spectrometry, Anal. Chem. 91 (2019) 6353–6362.
[19] Y.H. Zhang, Y.Y. Song, J. Wu, R.J. Li, D. Hu, Z.A. Lin, Z.W. Cai, A magnetic covalent organic framework as an adsorbent and a new matrix for enrichment and rapid determination of PAHs

and their derivatives in $PM_{2.5}$ by surface-assisted laser desorption/ionization-time of flight-mass spectrometry, Chem. Commun. 55 (2019) 3745–3748.

[20] M. Fischnaller, R. Köck, R. Bakry, G.K. Bonn, Enrichment and desalting of tryptic protein digests and the protein depletion using boron nitride, Anal. Chim. Acta 823 (2014) 40–50.

[21] R. El Kurdi, D. Patra, Amplification of resonance Rayleigh scattering of gold nanoparticles by tweaking into nanowires: Bio-sensing of α-tocopherol by enhanced resonance Rayleigh scattering of curcumin capped gold nanowires through non-covalent interaction, Talanta 168 (2017) 82–90.

[22] M. Qasem, R. El Kurdi, D. Patra, F108 stabilized CuO nanoparticles for highly selective and sensitive determination of mercury using resonance Rayleigh scattering spectroscopy, Anal. Methods 12(2020) 2133–2142.

[23] Z. Zhao, C.N. Bai, L.L. An, X.F. Zhang, F. Wang, Y. Huang, M.N. Qu, Y.L. Yu, Biocompatible porous boron nitride nano/microrods with ultrafast selective adsorption for dyes, J. Environ. Chem. Eng. 9 (2021) 104797.

[24] Z. Li, Y.H. Zhang, C. Chan, C.Y. Zhi, X.L. Cheng, J. Fan, Temperature-dependent lipid extraction from membranes by boron nitride nanosheets, ACS Nano 12 (2018) 2764–2772.

[25] S. Roy, X. Zhang, A.B. Puthirath, A. Meiyazhagan, S. Bhattacharyya, M.M. Rahman, G. Babu,; S.K. Saju, M.K. Tran, L.M. Sassi, M.A.S.R. Saadi, J. Lai, O. Sahin, S.M. Sajadi, B. Dharmarajan, D. Salpekar, N. Chakingal, A. Baburaj, X. Shuai, A. Adumbumkulath, K.A. Miller, J.M. Gayle, A. Ajnsztajn, T. Prasankumar, V.V.J. Harikrishnan, V. Ojha, H. Kannan, A.Z. Khater, Z. Zhu, S.A. Iyengar, P.A.d.S. Autreto, E.F. Oliveira, G. Gao, J. Taha-Tijerina, R.M. Yadav, S. Arepalli, R. Vajtai, P.M. Ajayan, Structure, properties and applications of two-dimensional hexagonal boron nitride, Adv. Mater. (2021) 2101589.

[26] A.U. Ahmad, H.W. Liang, S. Ali, Q. Abbas, A. Farid, A. Ali, M. Iqbal, I. Ahmad khan, L.J. Pan, A. Abbas and Z. Farooq, Cheap, reliable, reusable, thermally and chemically stable fluorinated hexagonal boron nitride nanosheets coated Au nanoparticles substrate for surface enhanced Raman spectroscopy, Sens. Actuators B 304 (2020) 127394.

[27] Y.X. Zhao, Z.Y. Sui, Z.S. Chang, S.L. Wang, Y. Liang, X. Liu, L.J. Feng, Q. Chen, N. Wang, A trifluoromethyl-grafted ultra-stable fluorescent covalent organic framework for adsorption and detection of pesticides, J. Mater. Chem. A 8 (2020) 25156–25164.

[28] X.M. Li, S.J. Dong, W. Zhang, X. Fan, R.G. Wang, P.L. Wang, X.O. Su, The occurrence of perfluoroalkyl acids in an important feed material (fishmeal) and its potential risk through the farm-to-fork pathway to humans, J. Hazard. Mater. 367 (2019) 559–567.

[29] Y.Y. Lu, X.L. Wang, L.L. Wang, W. Zhang, J.J. Wei, J.M. Lin, R.S. Zhao, Room-temperature synthesis of amino-functionalized magnetic covalent organic frameworks for efficient extraction of perfluoroalkyl acids in environmental water samples, J. Hazard. Mater. 407 (2021) 124782.

[30] B. Sha, J.H. Johansson, J.P. Benskin, I.T. Cousins, M.E. Salter, Influence of water concentrations of perfluoroalkyl acids (PFAAs) on their size-resolved enrichment in nascent sea spray aerosols, Environ. Sci. Technol. 55 (2021) 9489–9497.

[31] F. Vela-Soria, J. Garcia-Villanova, V. Mustieles, T. de Haro, J.P. Antignac, M.F. Fernandez, Assessment of perfluoroalkyl substances in placenta by coupling salt assisted liquid-liquid extraction with dispersive liquid-liquid microextraction prior to liquid chromatography-tandem mass spectrometry, Talanta 221 (2021) 121577.

[32] Y.F. Huang, W.H. Zhang, M.D. Bai, X.J. Huang, One-pot fabrication of magnetic fluorinated carbon nanotubes adsorbent for efficient extraction of perfluoroalkyl carboxylic acids and perfluoroalkyl sulfonic acids in environmental water samples, Chem. Eng. J. 380 (2020) 122392.

[33] P.W. Wu, W.S. Zhu, Y.H. Chao, J.S. Zhang, P.F. Zhang, H.Y. Zhu, C.F. Li, Z.G. Chen, H.M. Li, S Dai, A template-free solvent-mediated synthesis of high surface area boron nitride nanosheets for aerobic oxidative desulfurization, Chem. Commun. 52 (2016) 144–147.

[34] M. Du, X.L. Li, A.Z. Wang, Y.Z. Wu, X.P. Hao, M.W. Zhao, One-step exfoliation and fluorination of boron nitride nanosheets and a study of their magnetic properties, Angew. Chem. Int. Ed. 53 (2014) 3645–3649.

[35] J.K. Li, Y.Y. Gao, Y.Q. Wan, J.H. Liu, L. Liu, J.H. Wang, X.L.; Sun, F.W. Pi, X.F. Chen, A novel analytical strategy for the determination of perfluoroalkyl acids in various food matrices using a home-made functionalized fluorine interaction SPME in combination with LC-MS/MS, Food Chem. 366 (2022) 130572.

[36] S. Radhakrishnan, D. Das, A. Samanta, C.A. de los Reyes, L.Z. Deng, L.B. Alemany, T.K. Weldeghiorghis, V.N. Khabashesku, V. Kochat, Z.H. Jin, P.M. Sudeep, A.A. Martí, C.W. Chu, A. Roy, C.S. Tiwary, A.K. Singh, P.M. Ajayan, Fluorinated h-BN as a magnetic semiconductor, Sci. Adv. 3(2017) 1700842.

[37] Y.Q. Bai, J. Zhang, Y.F. Wang, Z.Y. Cao, L.L. An, B. Zhang, Y.L. Yu, J.Y. Zhang, C.M. Wang, Ball milling of hexagonal boron nitride microflakes in ammonia fluoride solution gives fluorinated nanosheets that serve as effective water-dispersible lubricant additives, ACS Appl. Mater. Interfaces 2 (2019) 3187–3195.

[38] Y.J. Zhao, Q.B. Liao, K. Xi, D.K. Xu, MoS_2-assisted LDI Mass spectrometry for the detection of small molecules and quantitative analysis of sulfonamides in serum, J. Am. Soc. Mass Spectrom. 32 (2021) 2463–2471.

[39] Y.M. Yang, W.H. Niu, W.Q. Wang, S.Y. Qi, L.L. Tong, X.Y. Mu, Z.Z. Chen, W.F. Li, B. Tang, h-FBN assisted negative ion paper spray for the sensitive detection of small molecules, Chem. Commun. 57 (2021) 6612–6615.

[40] X. Huang, Q. Liu, X.Y. Huang, Z. Nie, T. Ruan, Y.G. Du, G.B. Jiang, Fluorographene as a mass spectrometry probe for high-throughput identification and screening of emerging chemical contaminants in complex samples, Anal. Chem. 89 (2017) 1307–1314.

Figure Captions

Fig. 1: Scheme illustrating the synthesis of F-BNNs and the analysis of PFAAs in complex samples by MALDI MS and MSI using the F-BNNs as an adsorbent and matrix.

Fig. 2: (a) SEM and (b) TEM images of F-BNNSs; (c) survey XPS spectrum and high-resolution spectra of the (d) F 1s, (e) B 1s, and (f) N 1s spectra of F-BNNs; (g) XRD patterns and (h) FT-IR spectra of BNNs and F-BNNs; (i) N_2 adsorption (green line)-desorption (red line) isotherm of F-BNNs, and its pore size distribution (inset).

Fig. 3: Mass spectra of PFAAs obtained using (a) F-BNNs, (b) BNNs, (c) CHCA, (d) DHB, (e) GO, (f) GS matrices. Each analyte concentration was set at 10 μg L^{-1}.

Fig. 4: Salt tolerance of F-BNNs matrix (a). Mass spectra of blank human serum sample with F-BNNs as enrichment and ionization material without (b), and with (c) spiked with PFAAs. MALDI-MSI analysis of PFAA distribution in zebrafish using the F-BNN matrix; 1-Eyes, 2-Liver, 3-Sexual organs, 4-Anus, 5-End of sex organ; (01) Fish model, Different PFAA molecules of (02) m/z 299.10, (03) m/z 399.11, (04) m/z 499.13, and (05) m/z. 512.94 distribution in zebrafish.

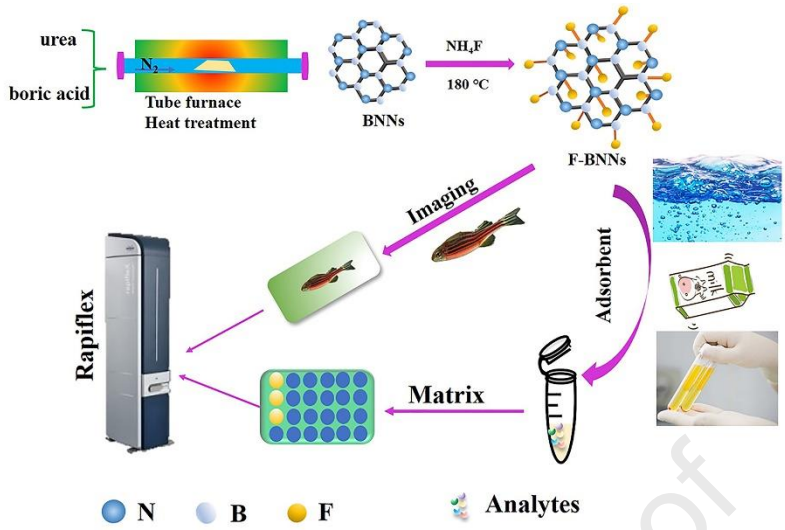

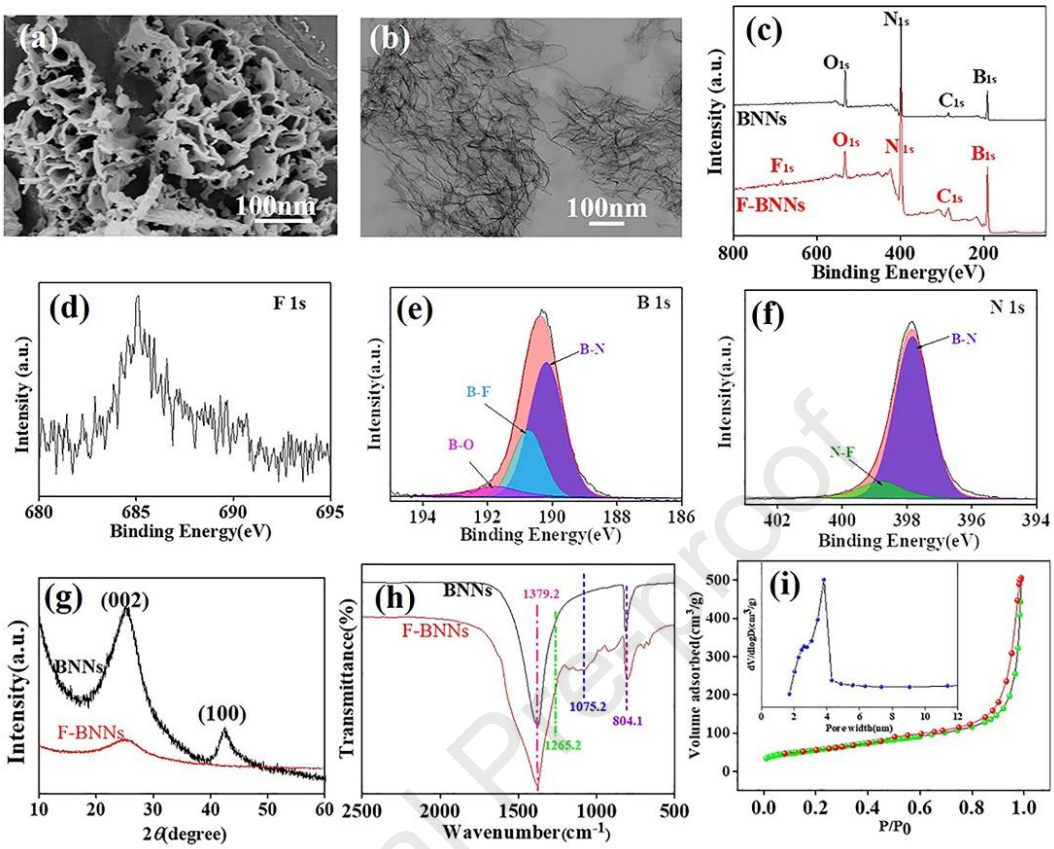

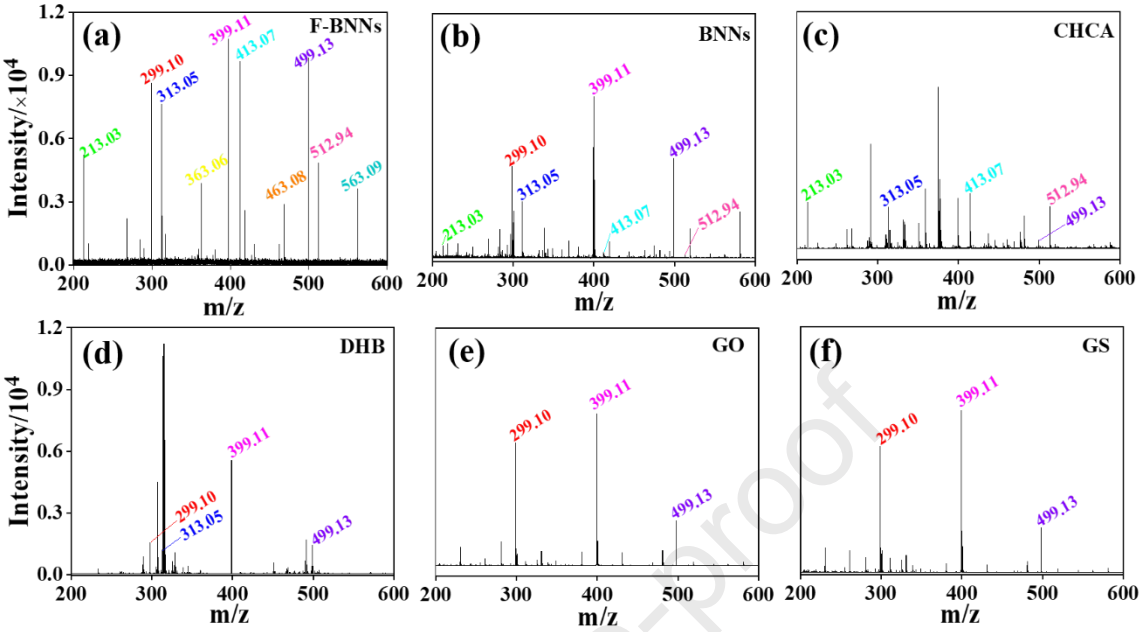

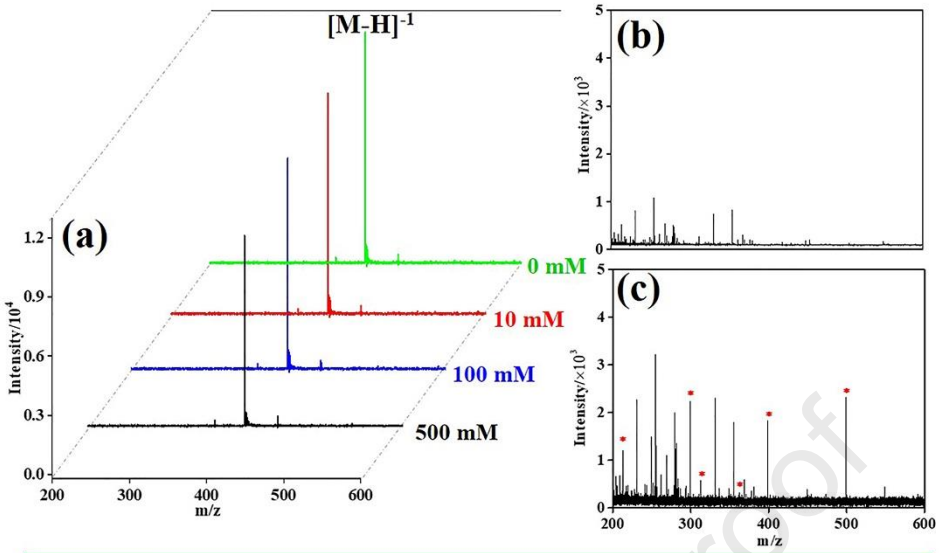

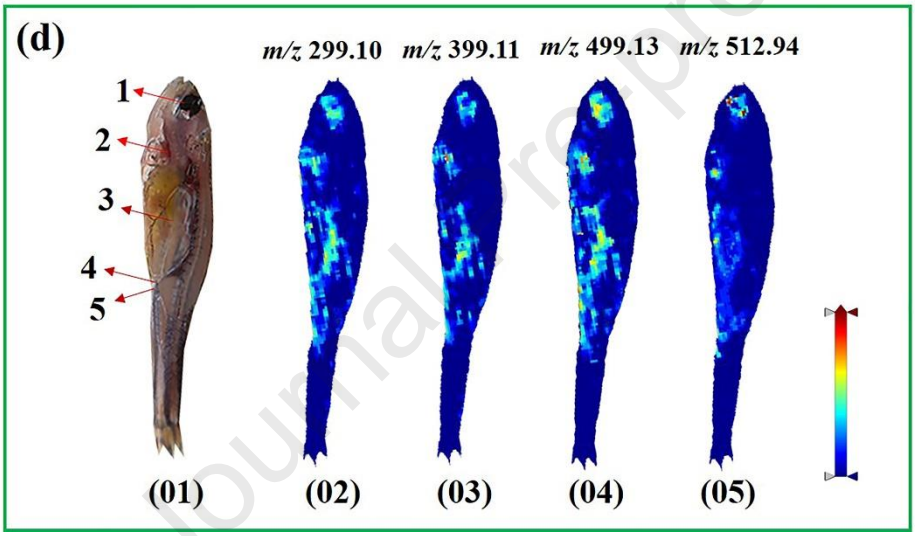

Highlights

- F-BNNs was used as absorbent and inorganic matrix for MALDI-MS analysis of PFAAs in water, milk, and human serum samples.
- Mass imaging of PFAAs in zebrafish was explored using F-BNNs.
- The possible ionization mechanism of F-BNNs as matrix was discussed.

Declaration of competing interest

The authors declare that they have no known competing financial interests or personal relationships that could have appeared to influence the work reported in this paper.